EM-HyChem: Bridging molecular simulations and chemical reaction neural network-enabled approach to modelling energetic material chemistry

Xinzhe Chen[a], Yabei Xu[a], Mingjie Wen[a], Kehui Pang[a], Shengkai Wang[b], Qingzhao Chu[a], Dongping Chen[a,*]

[a] *State Key Laboratory of Explosion Science and Technology, Beijing Institute of Technology, Beijing 100081, China*

[b] *State Key Laboratory of Turbulence and Complex Systems, College of Engineering, Peking University, Beijing 100871, China*

*Corresponding Author: Dongping Chen
E-mail address: dc516@bit.edu.cn

Abstract

This study introduced a physics-inspired, top-down approach for modelling the reaction kinetics of energetic materials, based on observations of the time scale separation between pyrolysis and oxidation reactions. This modelling approach, named EM-HyChem, was developed with the inspiration of the original hybrid chemistry (HyChem) model, in which the reaction mechanism is divided into two submodels: pyrolysis and oxidation. In EM-HyChem, the key pyrolysis products and reaction mechanism are identified from the perspective of molecular fragments via geometry analysis, which is validated via neural network potential-enabled molecular dynamic simulations. A chemical reaction neural network (CRNN) model is applied to extract the rate parameters for the pyrolysis step from the reproduction of thermogravimetric experiments. An EM-HyChem model is later constructed by combining the pyrolysis step together with the oxidation models for the pyrolysis products. Two representative EMs, i.e., 1,3,5-trinitroperhydro-1,3,5-triazine (RDX) and 1,3,5,7-tetranitro-1,3,5,7-tetrazocane (HMX), are considered here to evaluate the performance of the EM-HyChem model. The predicted burning rates across a wide range of pressure conditions (1–100 atm) are in good agreement with the experimental measurements and the results of other models. Further agreement among the temperate profile, melt layer thickness and surface temperatures support the EM-HyChem model.

Keywords: energetic materials; neural network potential; chemical reaction neural network; kinetic model; burning rate

1. Introduction

Energetic materials (EMs) are a class of chemical substances that are capable of releasing significant quantities of energy during decomposition [1, 2]. The high-energy properties of EMs have led to a diverse range of applications in the national defense and aerospace industries [3]. The combustion characteristics of EMs, such as their burning rate, determine their practical performance as solid propellants [4-8]. A comprehensive understanding of the thermal decomposition process and the kinetic behavior of EMs is essential for evaluating their combustion characteristics. It is therefore imperative to gain an in-depth understanding of their reaction kinetics, facilitating the design, preparation and safety assessment of such materials.

Since the 1970s, thermogravimetric (TG) analysis and differential scanning calorimetry (DSC) techniques have been employed extensively in thermal decomposition experiments of EMs with the aim of elucidating the underlying reaction kinetics [9, 10]. Considering two representative EMs, i.e., 1,3,5-trinitroperhydro-1,3,5-triazine (RDX) and 1,3,5,7-tetranitro-1,3,5,7-tetrazocane (HMX), many experimental works have been applied to tackle their decomposition kinetics. Lee et al. [11] employed TG analysis to investigate the thermal decomposition process of HMX. Their findings revealed that HMX undergoes a crystalline transformation and melting prior to the onset of decomposition, which subsequently proceeds through a series of decompositions. Wang et al. [12] investigated the thermal decomposition of HMX via DSC, identifying the endothermic peak for HMX melting at 553 K and the exothermic decomposition at 558 K. Khichar et al. [13] carried out simultaneous thermal experiments on RDX via TG-DSC-FTIR and reported that the thermal decomposition of RDX produced gaseous products such as HCHO, HCN, N_2O, CO_2, H_2O, CO, NO and NO_2. These experiments provide a variety of fruitful data for kinetic models to interpret the thermal decomposition of EMs. The representative kinetic models include the Kissinger [14], Ozawa [15], Friedman [16] and Starink models [17]. Lee et al. [11] employed the Kissinger model to analyse the DSC data of RDX, thereby deriving an apparent activation energy of ~144 kJ/mol. Fathollahi et al. [18] tested RDX simultaneously via thermogravimetry differential thermal analysis (TG-DTA) and DSC under nonisothermal conditions. They determined that the activation energy of RDX decomposition with different particle sizes ranged from 161.1-272.5 kJ/mol via both the Kissinger and Ozawa models. Jiao et al. [19] calculated the TG data of RDX/AP via the Friedman model and reported that the apparent activation energy of the low-temperature decomposition process is negative, indicating that RDX is highly susceptible to deflagration in the presence of AP. Tang et al. [20] calculated the TG data of nitrocellulose at different oxygen contents via the Starink model, and the activation energy ranged from 160 to 375 kJ/mol. These available models are analogous to one-step global reactions that serve as good tools to evaluate the reactivity of EMs under thermal stimuli. However, the models themselves cannot be extended to predict any time-resolved and species-dependent combustion characteristics, limiting their

applications in practical cases.

Unlike one-step kinetic models, Patidar et al. [21] constructed a reaction kinetic model with elementary reactions that is capable of describing HMX decomposition at the condensed phase via experiments and density functional theory (DFT) calculations. This kinetic model includes 109 species and 157 reactions, and the mass loss in TG experiments can be well reproduced. However, the development of the above models with elementary reactions requires a significant workload and scientific intuition, not to mention the fine experimental apparatus used to determine the kinetic characteristics. As a result, only a handful of kinetic models for EMs are available, despite the poor transferability of the kinetic model. In contrast to the dilemmas in the development of reaction models for EMs, the combustion community has made tremendous efforts to combine advanced diagnostic methods with highly accurate theoretical calculations for the reaction mechanism of hydrocarbon fuels [22, 23]. In the last decade, one of the most significant works is the establishment of the HyChem approach [24-26]. This approach embeds a physically guided approximation, i.e., separation of scales, to divide the fuel combustion process at high temperatures into two subprocesses: pyrolysis and oxidation of the pyrolysis products. The HyChem approach has been applied to describe the combustion of conventional jet fuels (JP-8, Jet A and JP-5) and rocket fuels (RP2-1 and RP2-2) [27]. In HyChem models, a "one-species" fuel pyrolysis model is parameterized to describe fuel pyrolysis and radical-assisted pyrolysis according to experimental measurements, whereas the oxidation component is represented via a detailed foundation fuel chemistry model. The above treatment masters the critical physics behind combustion kinetics and reduces the model complexity by combining lumped steps with elementary reactions. A HyChem-like strategy could be a feasible approach to resolve the unknown kinetics in EMs.

In recent years, with the advent of computational technology, novel techniques, such as machine learning, have been increasingly employed in the modelling of reaction kinetics in EMs [28]. The training process of machine learning involves the extraction of underlying patterns from datasets through the establishment of connections with a trained model. This enables the generation of predictions or decisions on the basis of the analysis of new data [29]. For example, Green et al. [30] devised a graph-convolution neural network for encoding a reduced map of reactions, which was then employed to successfully predict reaction enthalpies, rate constants, and reaction classes. Nevertheless, the lack of a physical interpretation of the reaction model and the inability to elucidate the reaction process represent significant limitations. To address this limitation, Deng et al. [31] proposed a chemical reaction neural network (CRNN) for the autonomous discovery of reaction pathways, which is capable of identifying reaction pathways and optimizing kinetic parameters from the evolution of species concentration or mass loss without any prior knowledge of the reaction mechanism. Compared with traditional kinetic models [14-17] and detailed reaction models [32], the CRNN model [33] markedly enhances computational efficiency while ensuring computational accuracy. In terms of transferability, the CRNN model has demonstrated

its potential to resolve the thermal decomposition of EMs under different heating rates [33-35]. However, the CRNN model is not suitable for the direct prediction of combustion characteristics, such as the burning rate of EMs.

Considering all the previous efforts in tackling the mysterious reaction kinetics of EMs, the available modelling methods are constrained by several inherent limitations, including poor transferability, high development cost and even unphysical interpretation. An alternative approach that can combine these advantages, such as the simplicity of one-step lumped reactions, the transferability of elementary reactions and the low development cost of data-driven methods, regardless of their inherent drawbacks, is desirable. In this work, a method termed the "EM-HyChem" approach is proposed to build a kinetic framework for EMs on the basis of the HyChem approach. The model encompasses a lumped pyrolysis mechanism together with a detailed oxidation mechanism for the pyrolysis products. To simplify the pyrolysis step, the molecular dynamics (MD) method is employed to identify key products and reaction pathways for three representative EMs, i.e., RDX, HMX and CL-20. The CRNN is then employed to extract the kinetic parameters from the interpretation against the mass loss in TG experiments. The EM-HyChem model is constructed by further combining the detailed oxidation mechanism of the pyrolysis products. The model predictions of the combustion properties, such as the burning rates of RDX and HMX, are validated via a classical three-phase combustion model against experimental data.

2. Methodology

A 1D combustion model was constructed to evaluate the burning rates of RDX and HMX in the present work. Figure 1 depicts the structure of the three-phase combustion model for RDX, which is consistent with the model proposed in previous works [4-6]. The one-dimensional model is divided into three phases: a solid layer, a melt (liquid) layer, and a gas layer [36-38]. The model is developed in a reference system on the burning surface, and the position of the liquid–gas interface remains unchanged. The objective of the model calculations is to predict the burning rates of solid materials by solving the governing equations for energy and kinetics.

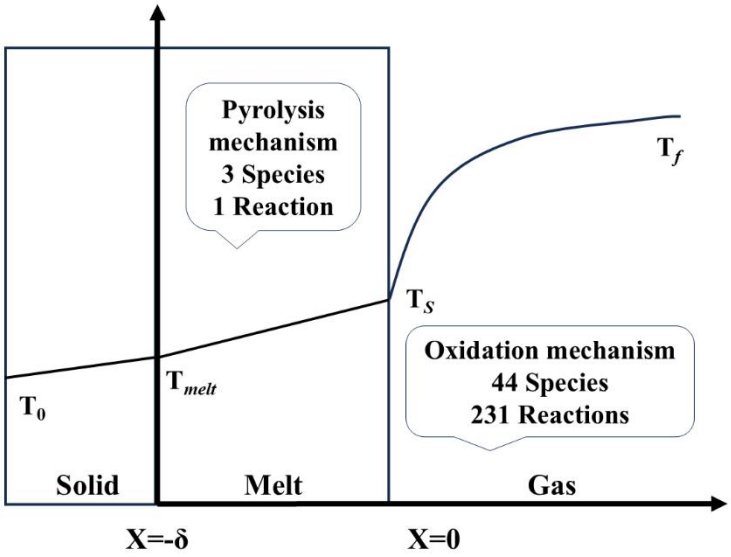

Figure 1. Schematic of the three-phase combustion model for self-deflagration of RDX. δ is the thickness of the melt layer. T_0, $T_{\underline{\text{melt}}}$, T_S and T_f represent the temperatures of the initial stage, melting point, liquid–gas interface and flame, respectively. The mechanism size is taken from the complied EM-HyChem model for RDX.

In the solid layer, the slow reaction rate is negligible, and the energy equation is solved via Eq. (1):

$$\dot{m}^{"} C_p \frac{dT}{dx} = \frac{d}{dx}(\lambda \frac{dT}{dx}), \tag{1}$$

where $\dot{m}^{"}$ is the mass flux rate, C_p is the specific heat of the solid layer, T is the temperature, and λ is the thermal conductivity in the solid layer. Once the material melts, a liquid layer is formed where the material begins to thermally decompose under pyrolysis. The liquid layer is represented as a liquid solution containing dissolved gas, assuming negligible mass diffusion within the liquid layer. The governing equations in the liquid phase are expressed below:

$$\dot{m}^{"} \frac{dY_k}{dx} = \dot{\omega}_k W_k, \tag{2}$$

$$\dot{m}^{"} C_p \frac{dT}{dx} = \frac{d}{dx}(\lambda \frac{dT}{dx}) - \sum_{k=1}^{n} \dot{\omega}_k h_k W_k, \tag{3}$$

where k represents the kth substance in the liquid, Y_k is the mass fraction, $\dot{\omega}_k$ is the molar production rate, W_k is the molecular weight, and h_k is the enthalpy. The molar production rate is controlled by the pyrolysis model. For example, a previous work included 109 species and 157 reactions to resolve the pyrolysis kinetics of HMX decomposition [21]. In this work, we use a one-step pyrolysis model for RDX/HMX decomposition to yield NO_2 and CH_2N. The rationale for this pyrolysis model will be

explained in a later section.

In the gas layer, a set of governing equations is developed:

$$\rho = \frac{p\bar{W}}{RT}, \tag{4}$$

$$\dot{m}'' \frac{dY_k}{dx} = -\frac{d}{dx}(\rho Y_k V_k) + \dot{\omega}_k W_k, \tag{5}$$

$$\dot{m}'' C_p \frac{dT}{dx} = \frac{d}{dx}(\lambda \frac{dT}{dx}) - \sum_{k=1}^{n} \dot{\omega}_k h_k W_k - \sum_{k=1}^{n} \rho Y_k v_k C_{pk} \frac{dT}{dx}, \tag{6}$$

where ρ is the mass density, p is the pressure, $\bar{W}$ is the average molecular weight, R is the universal gas constant, v_k is the diffusion velocity, and C_{pk} is the specific heat of the first substance in the gas layer. The gas-phase kinetic model describes the oxidation reaction process of NO_2 and CH_2N. The Cantera [39] solver is employed here to simulate the aforementioned chemical dynamics under steady-state conditions.

The mass flux rate $\dot{m}''$ is calculated iteratively between the liquid and gas layers. The mole fraction of surface matter in the liquid layer is provided as an input to the gas layer. The mass balance at the liquid–gas interface is automatically satisfied, and the energy balance at the interface determines the mass flux rate $\dot{m}''$:

$$\left[\dot{m}'' \sum_{k=1}^{n} Y_k h_k - \lambda \frac{dT}{dx}\right]_{liquid} = \left[\dot{m}'' \sum_{k=1}^{n} Y_k h_k - \lambda \frac{dT}{dx}\right]_{gas}, \tag{7}$$

An empirical equation for pyrolysis, analogous to the Arrhenius formula, is employed at the liquid–gas interface to delineate the interrelationship between the surface temperature T_S and the mass flux rate $\dot{m}''$ [36, 40-42]:

$$\dot{m}'' = m_0 \exp(-E_S / RT_S), \tag{8}$$

where E_S is the surface activation energy (cal/mol) and m_0 is a constant (g/cm^2·s^{-1}). Both are fitted by the experimental data of Zenin [43-45]. All the parameters involved in the combustion model are given in Table S1. The burning rate r_b of the solid materials is calculated for a given pressure according to the following formula:

$$r_b = \frac{\dot{m}''}{\rho} \tag{9}$$

3. Decomposition of RDX and HMX

3.1 Molecular simulation of pyrolysis reactions

According to recent MD studies of RDX and HMX decomposition [46], the major decomposition intermediates and products are the same, including NO_2, NO, H_2O, N_2 and CO_2, and the corresponding time histories of the above species are nearly identical. Another US research team reported that RDX and HMX decomposition yield the same number of products per unit mass basis via MD simulations (Figure 8 in ref. [47]). Both works considered an in-house neural network reactive force field to support the MD simulations, and the same phenomenon was identified independently. The above phenomenon raises the question of why RDX and HMX have different molecular structures but have the same pyrolysis characteristics.

To resolve the above question, we hypothesized that the reaction kinetics of RDX and HMX are similar to those of their molecular fragments, i.e., $CH_2N\text{-}NO_2$ or, more aggressively, CH_2N and NO_2 (i.e., CH_2N+NO_2). This study innovatively introduces a molecular fragment model to evaluate the pyrolysis mechanisms of RDX and HMX. The inspiration for this hypothesis comes from the molecular structures of RDX and HMX because they can both be represented as $(CH_2N\text{-}NO_2)_3$ and $(CH_2N\text{-}NO_2)_4$, respectively. Additionally, CL-20, which has a $(CHN\text{-}NO_2)_6$ structure, is included in a comparative study to further evaluate the above approximation.

Geometric analysis revealed that the internal C–N and C–C bonds of RDX and HMX molecules are broken (Figure 2), leading to the decomposition of RDX and HMX into three and four $CH_2N\text{-}NO_2$ fragments, respectively. NO_2 is the major intermediate in the decomposition of RDX and HMX [32, 48]. Further breakage of the N–N bond in $CH_2N\text{-}NO_2$ fragments generates CH_2N and NO_2. Therefore, both RDX and HMX molecules can be simplified to a structure of $(CH_2N+NO_2)_n$ (n = 3, 4). The above operations on molecular structures provide a possible reason for the same pyrolysis characteristics of RDX and HMX observed in MD simulations [47]. In contrast, the CL-20 molecule yields six $CHN\text{-}NO_2$ fragments via C–N and C–C bond scission, and further breakage of the N–N bond results in the formation of six CHNs and six NO_2 molecules. Instead, we can approximate CL-20 as a $(CHN+NO_2)_6$ structure.

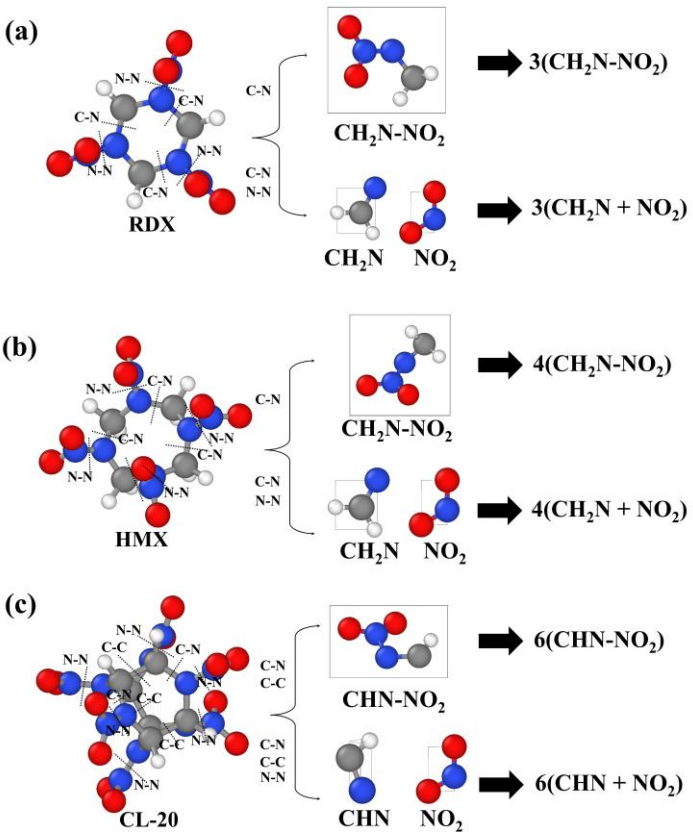

Figure 2. Disruption of C–N, C–C and N–N bonds in the structures of (a) RDX, (b) HMX and (c) CL–20 to form fragment units, i.e., CH_2N-NO_2, CHN-NO_2, CH_2N, CHN and NO_2. The blue, red, gray and white atoms represent nitrogen, oxygen, carbon, and hydrogen, respectively.

In this work, state-of-the-art neural network potential (NNP)-enabled MD simulations are applied to evaluate the decomposition characteristics of RDX, HMX and CL-20 via the above molecular fragments. The corresponding structures, which consist of both the complete molecules and the fragment units, are shown in Figure 3. Each RDX and CL-20 crystal structure is a 2×2×2 supercell containing 64 molecules, whereas the HMX crystal contains 16 molecules. The CH_2N-NO_2 and CHN-NO_2 units are named fragment model 1 (FM1). The initial structures composed of CH_2N and NO_2 for RDX and HMX and CHN and NO_2 for CL-20 are termed fragment model 2 (FM2). The initial model was built via Packmol [49], with molecular fragments randomly distributed throughout the system, maintaining the same density as RDX, HMX, and CL-20 crystals. The radial distribution functions (RDFs) of the initial geometry for the crystals and fragment units are included in Figure S1. According to the RDF results of the C–C pair, the results of the crystal case exhibit several clear peaks, whereas the results of the fragment model show no obvious peak at either short- or long-range distances, indicating the presence of amorphous structures.

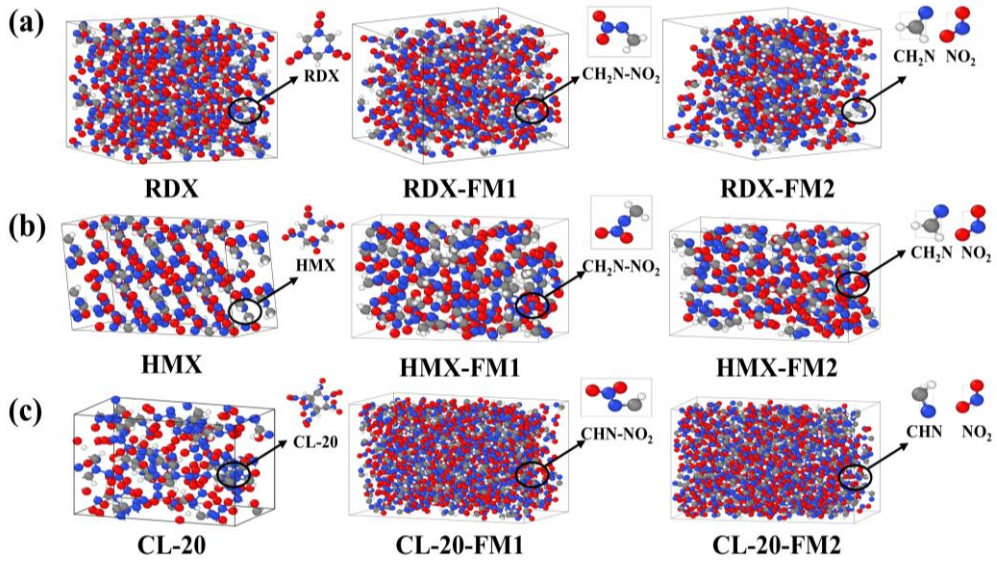

Figure 3. Initial models of (a) RDX, (b) HMX, and (c) CL-20, including molecules and fragment units (CH_2N-NO_2, CHN-NO_2, CH_2N, and CHN, NO_2).

Here, each case with fragment units first undergoes a 20 ps low-temperature relaxation at 300 K. The equilibrated structures are then simulated at a high temperature of 2000 K under the NVT ensemble for 100 ps to capture the pyrolysis kinetics. In Figure 4, the thermal decomposition processes of RDX, HMX, RDX-FM1, HMX-FM1, RDX-FM2 and HMX-FM2 exhibit notable similarities. In particular, the primary gaseous products of RDX and HMX crystals, i.e., H_2O and N_2, are rapidly formed within 0 to 25 ps and 0 to 40 ps, respectively. This is consistent with the findings of previous MD simulations, as RDX and HMX share almost the same decomposition characteristics [46, 47]. In addition, FM1 and FM2 also show the same trends as those of the crystal cases. For other species, such as NO, CO_2, and HNO_2, we can draw the same conclusion. Only exceptions can be observed before ~2 ps; for example, the case of the RDX crystal shows a peak of NO_2, whereas the FM2 cases exhibit a decay trend because NO_2 is one of the starting species in FM2. Overall, during the decomposition of RDX and HMX, whether in the form of intact molecules or different molecular fragment units, the evolution patterns of the types and quantities of intermediates and products over time present minor differences. This finding suggests that the decomposition rate of EM molecules during the pyrolysis stage is much faster than their oxidation rate. In the pyrolysis stage, the RDX and HMX molecules rapidly decompose into CH_2N and NO_2. The subsequent oxidation reactions are driven primarily by the oxidation of these two intermediates. Therefore, the pyrolysis process of EMs can be simplified into two stages: the pyrolysis of EM molecules into key intermediates and further oxidation of the intermediates. This is consistent with the core idea behind the original HyChem approach [24].

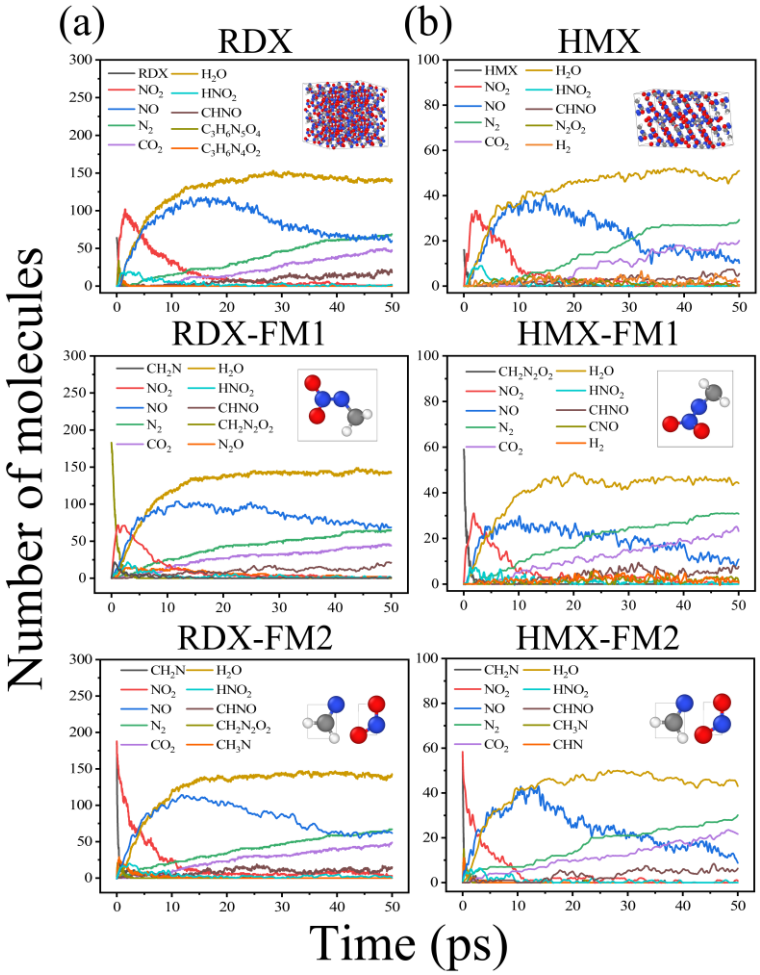

Figure 4. Evolution of decomposition products at 2000 K: (a) RDX and (b) HMX. The first, second and third rows represent the cases of the crystal, fragment model 1 (CH_2N-NO_2 unit), and fragment model 2 (CH_2N and NO_2 fragments), respectively.

In addition, the $(CHN\text{-}NO_2)_6$ structure of CL-20 is used as a reference to verify the rationality of the above-simplified method. In Figure 5, the results indicate that the CL-20 molecule and its fragment models follow a similar evolution pattern in terms of product type and formation order. For example, CL-20-FM1 and CL-20-FM2 produce the same product types observed in the case of the CL-20 crystal. Moreover, both models demonstrate a high degree of consistency in the patterns of product formation.

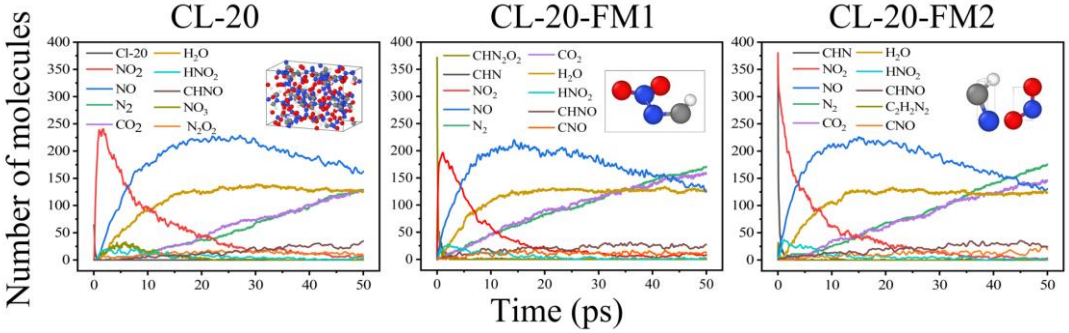

Figure 5. Distribution of decomposition products from the CL-20 crystal, fragment model 1 (CHN-NO_2 unit), and fragment model 2 (CHN and NO_2 fragments).

Considering the above cases of RDX, HMX and CL-20, we can thus approximate their pyrolysis via a single-step reaction as RDX/HMX => $CH_2N + NO_2$ and CL-20 => $CHN + NO_2$. This serves as an effective approximation for understanding their pyrolysis process. Therefore, the pyrolysis kinetics of the molecular fragment models elucidate the intrinsic mechanisms of the thermal decomposition of EMs.

3.2 Chemical reaction neural network-enabled pyrolysis modelling

The CRNN is employed to extract lumped pyrolysis reactions and the corresponding kinetic parameters by training against the experimental mass loss in TG measurements. Previous successful CRNN models for RDX [33], HMX [35], and CL-20 [34] have been developed. The potential intermediates and reaction pathways were inferred from experimental evidence or theoretical calculations [50, 51]. However, in this work, we impose a one-step pyrolysis pathway in the training of the CRNN model via the fragment model with CH_2N/CHN and NO_2. The thermogravimetric data of RDX [33], HMX [35] and CL-20 [34] were taken from previous measurements. Figure 6 shows the excellent reproduction of the experimental results obtained via the one-step pyrolysis reaction. The predicted curves yield relative errors of 0.027, 0.017, and 0.02 for RDX, HMX and CL-20, respectively. The kinetic parameters of all three one-step pyrolysis models are shown in Table 1. Figure S2 shows the mass evolution of RDX, HMX and CL-20 and describes the distribution of the main pyrolysis products, i.e., CH_2N, CHN and NO_2.

Table 1. Pyrolysis reactions and kinetic parameters of RDX, HMX and CL-20

Reaction	E_a (cal/mol)	n	A (cm^3/mol/s)
RDX => $3CH_2N + 3NO_2$	46270.97	0.53	3.4856e+16
HMX => $4CH_2N + 4NO_2$	78446.58	1.11	3.4397e+25
CL-20 => $6CHN + 6NO_2$	59579.35	0.53	5.1847e+21

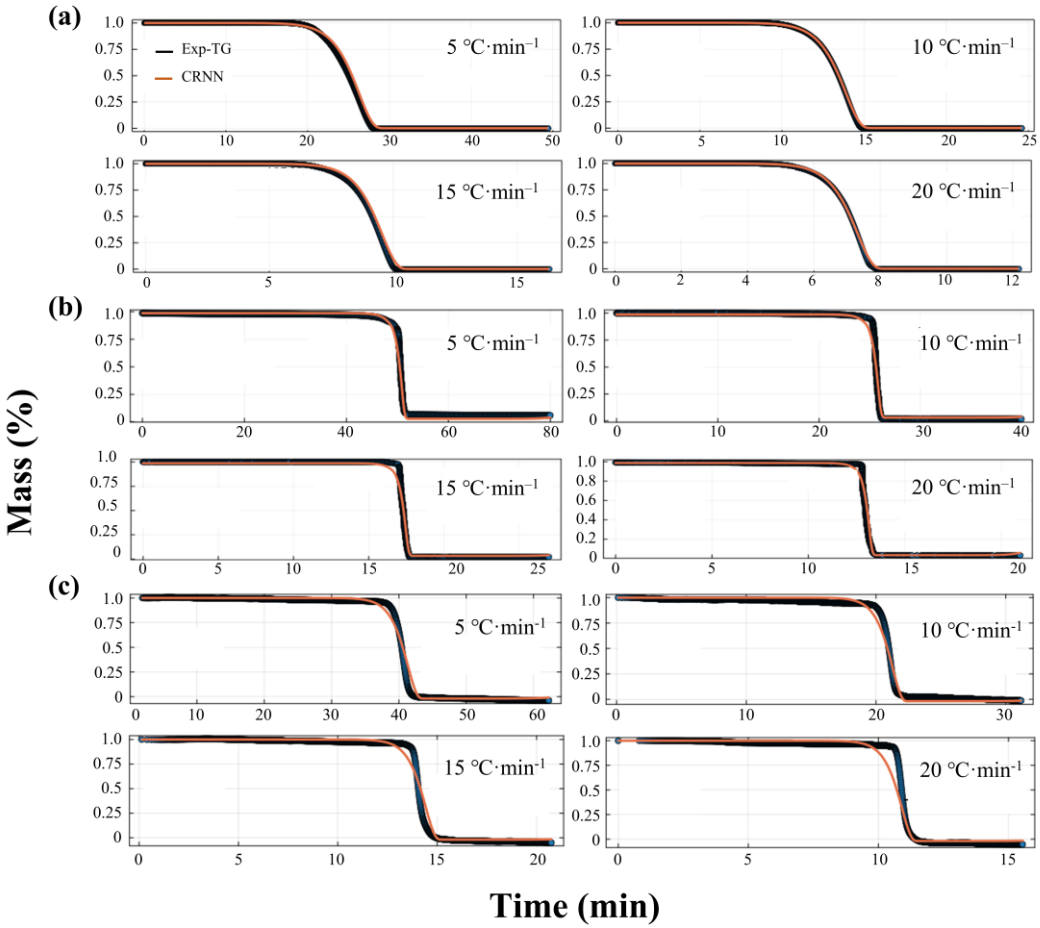

Figure 6. Predicted TG curves and experimental results for (a) RDX, (b) HMX, and (c) CL-20. The orange line and blue dots represent the predicted results from the CRNN models and experimental measurements, respectively.

4. The EM-HyChem approach

From the above molecular simulations of RDX, HMX and CL-20 combined with the CRNN approach, the complex decomposition mechanism is built by a one-step lumped reaction, representing a global, fast and path-insensitive solution. This provides a solid basis for combining the HyChem approach with an efficient and easy-to-apply kinetic model that can simulate the critical combustion characteristics of EMs. The above framework is termed the "EM-HyChem" approach (Figure 7). In contrast to the original HyChem approach [24], the pyrolysis model is not constrained by the fundamental combustion characteristics of the fuel, such as the ignition delay or speciation profile. Instead, state-of-the-art NNP-enabled MD simulations are applied to identify the molecular fragments that replace the detailed pyrolysis process. Here, we discuss the key assumptions and demonstrate the successful application of the current method for nitramine explosives (RDX, HMX and CL-20). In addition, the potential of the EM-HyChem approach for composites requires further evaluation compared with the known success of the original HyChem approach for practical fuels, i.e., Jet A [24], rocket fuels [25] and bioderived jet fuels [27].

The key assumptions are listed below:

(1) Energetic molecules include molecular fragments representing both fuel and oxidizers. They can be approximated as premixed mixtures at the molecular level.
(2) The oxidation step is far slower than the pyrolysis step. High-temperature MD simulations driven by the thermodynamic limit can reproduce the key molecular fragments involved in decomposition well.
(3) The number of molecular fragments needed to describe pyrolysis is substantially smaller than that needed to describe the corresponding energetic molecules. The complexity of a molecule is highly reduced. For example, the decomposition of RDX and HMX can be replaced by the formation of CH_2N and NO_2 (Figure 4).
(4) The mass loss evolution from TG experiments is a good constraint for deriving the decomposition rate of the measured materials.
(5) The combined kinetic model must include a lumped model for fuel pyrolysis and a detailed oxidation model for the molecular fragments as the products of the lumped pyrolysis model.
(6) The composite can be treated as a separate decomposition to form the corresponding molecular fragments. This requires further verification considering simplified composites.

In this study, the EM-HyChem approach constructed by MD and the CRNN is employed to overcome the limitations of traditional methods and to build pyrolysis models of EMs with greater efficiency and accuracy. This approach provides a theoretical framework for understanding the combustion behavior of EMs.

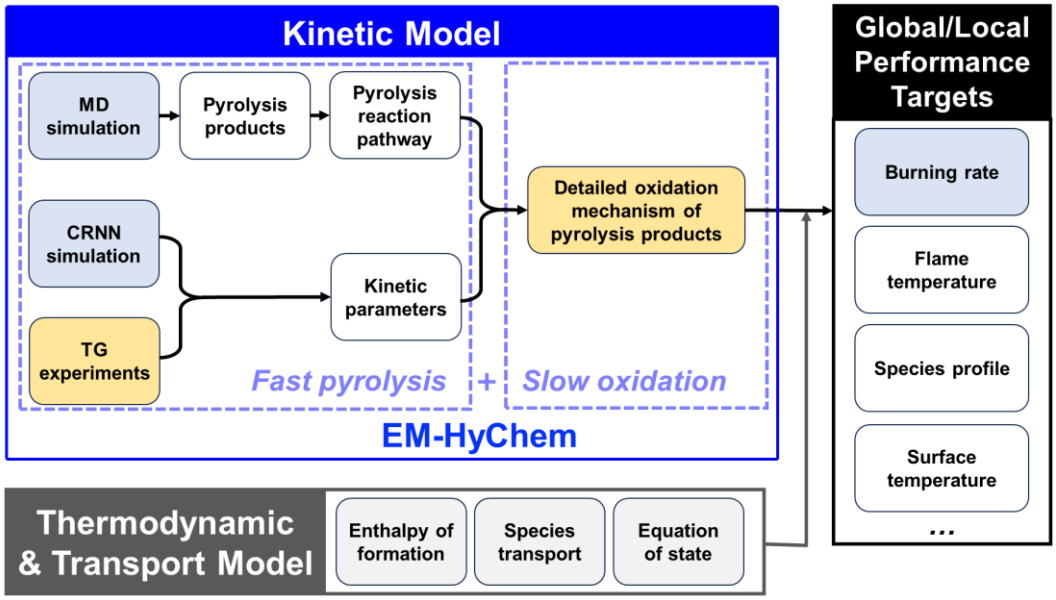

Figure 7. Schematic diagram of the EM-HyChem approach.

4.1 Lumped fuel pyrolysis model and oxidation model

The chemical formulas for both RDX and HMX are represented by $C_nH_{2n}N_{2n}O_{2n}$. The EM-HyChem model employs a one-step pyrolysis reaction to mimic the thermal decomposition of EMs:

$$RDX \rightarrow 3CH_2N+3NO_2, \quad (10)$$

$$HMX \rightarrow 4CH_2N+4NO_2. \quad (11)$$

Reactions 1 and 2 indicate that RDX and HMX molecules undergo N-NO_2 bond breakage on their side chains, followed by ring opening (C–N fission) of the primary ring, resulting in the formation of CH_2N and NO_2 small molecules. The kinetic parameters of reactions 1 and 2 are taken from thermogravimetric experiments using a CRNN (Table 1). The oxidation model of pyrolysis products, i.e., NO_2 and CH_2N, is treated via gas-phase elementary reactions [52, 53]. The gas-phase elementary reactions also include the gas-phase decomposition reactions of RDX and HMX because not all RDX and HMX are consumed in the condensed phase reactions at pressures lower than ~10 atm (Figure S3).

4.2 Experiments

For experimental analysis, Zenin [44] employed a micro-thermocouple technique to examine the combustion wave structure and burning rates of RDX and HMX powders with particle sizes ranging from 20 μm to 50 μm in nitrogen environments ranging from 1 to 90 atm. Atwood et al. [8] measured the burning rates of large, high-purity bulk powders of RDX and HMX in a nitrogen atmosphere from 0.24 MPa to 345 MPa via the film cinematography technique. Homan et al. [54] employed absorption spectroscopy to obtain the burning rate of a 0.8 cm diameter RDX sample within an air environment comprising a pressure range of 1–2 atm. The above burning rate data for RDX and HMX are compiled as a reference to validate the predictive capabilities of the EM-HyChem model. In addition to the burning rate data, the surface temperature and melt layer thickness over a wide range of pressures are also considered in the model validation.

4.3 Previous model development

Liau [5], Prasad [6] and Davidson et al. [4] built 1D combustion models for RDX monopropellants to investigate the structure of combustion waves via a semiglobal condensed-phase reaction kinetics mechanism and a detailed gas-phase reaction kinetics mechanism. A three-phase combustion model comprising solid, liquid and gas was constructed by Liau et al. [5]. The selected condensed-phase and gas-phase kinetic mechanisms included 3 reactions for 8 substances and 178 reactions for 38 substances. On the basis of the combustion model, the temperature distribution of RDX spontaneous combustion under different pressures and the effect of pressure on the burning rate of RDX monopropellants were evaluated. The pressure exponent of the burning rate was also extracted from the numerical prediction as 0.83. Prasad et al. [6] revised the condensed-phase reaction mechanism originally proposed by Liau et al. [5]

and expanded the gas-phase kinetic mechanism to include 48 substances and 228 reactions. They subsequently predicted the temperature distribution of the autoignition process of RDX at 1 atm and the burning rate at varying pressures on the basis of the constructed combustion model. Their findings revealed that the burning rate is proportional to the 0.76 power of the pressure. Davidson et al. [4] modified the kinetic parameters of the condensed-phase decomposition of RDX and incorporated the evaporation process. In turn, the burning rate, surface temperature and melt layer thickness of RDX at varying pressures were well reproduced against experimental measurements [4-6].

In the case of HMX monopropellants, Patidar et al. [55] used a similar 1D three-phase combustion model as Liau [5] for RDX to study the propagation of HMX combustion waves. Unlike the three-step global reaction mechanism developed by Brill [56] and Thynell et al. [57], Patidar et al. [55] developed a detailed reaction mechanism for HMX decomposition in the condensed phase via density functional theory (DFT) and TGA/FTIR studies, which included 109 substances and 157 reactions [21]. The gas-phase kinetic mechanism was originally developed by Chakraborty et al. [58] through quantum mechanical calculations and consists of 89 species and 462 reactions. In a subsequent work, Patidar et al. [55] used a combustion model to analyse the temperature distribution and the dependence of the burning rate on pressure for the spontaneous combustion of HMX at 1 atm. As the predicted burning rates at high pressures were markedly higher than the experimental values (Patidar model 1 in Figure 8b), the gas-phase kinetic mechanism was revised to improve the burning rate (Patidar model 2 in Figure 8b). The updated mechanism contains 81 species and 278 reactions [52].

Although the Liau, Prasad and Davidson models can predict certain combustion properties of EMs, the semiglobal kinetic model in the condensed phase does not accurately capture the correct physicochemical processes. In addition, the detailed kinetic model constructed by Patidar is also limited by the high workload in model development and high computational costs. In this work, we demonstrate the advantages of the EM-HyChem model in terms of its effectiveness, simplicity and high transferability. To achieve these goals, a lumped pyrolysis mechanism, as suggested from the fragment model, is integrated with the detailed elementary reaction mechanism in the aforementioned models. In particular, the detailed condensed-phase reaction mechanism (109 substances and 157 reactions) [21] is replaced by Reaction 1, which involves only three substances and one reaction for HMX. For the gas-phase combustion mechanism of HMX, we use the updated mechanism from the Patidar website [52]. For the gas-phase combustion mechanism of RDX, we simplify the mechanism from Pitz et al. [53], which consists of 49 substances and 185 reactions. The simulation results of the EM-HyChem model are compared with those of the aforementioned models in terms of burning rates, surface temperatures and melt layer thicknesses.

4.4 Tests against burning rates of RDX and HMX

The burning rate represents the most critical property in solid propellant combustion. The pressure dependence of the burning rate is typically expressed as [36]:

$$r_b = ap^n, \tag{10}$$

where n is the pressure exponent of the burning rate and a is a constant.

Figure 8 presents a comparison of the predicted burning rates obtained at an initial temperature of 298 K with experimental data and all available numerical results. For both RDX and HMX, the predicted burning rates of the EM-HyChem model are in good agreement with the experimental data and the other numerical methods despite their simplicity in the pyrolysis step. The experimental data on the burning rate of RDX obtained by Zenin [44], Miller, Homan [54], and Atwood et al. [8] are fitted to obtain a value of 0.041 and a pressure exponent n of 0.82 via eq. (10). The Prasad model [6] and Davidson model [4] yield a of 0.043, n of 0.80, and a of 0.033, n of 0.87, respectively. The EM-HyChem model predicts a of 0.039 and n of 0.9, and both values are within 5% of the above counterparts. For the burning rates of HMX, the experimental values of a is 0.042, and n is 0.79 [8, 44]. Patidar model 1 [55] yield a of 0.044 and n of 0.94, and Patidar model 2 [52] reproduces a of 0.032 and n of 0.82. In comparison, the EM-HyChem model predicts a reduced a of 0.015 and a greater n of 1.04 because of the underprediction of burning rates in the moderate-pressure region (<10 atm). In particular, the burning rate under atmospheric conditions is underestimated by 30.7% compared with that of the Patidar Model 2. This is because the EM-HyChem model predicts a greater residual mass at the end of HMX pyrolysis at low pressures, which absorbs more heat during gas-phase decomposition. This results in lower overall heat release and, consequently, a lower predicted burning rate (Figure S3).

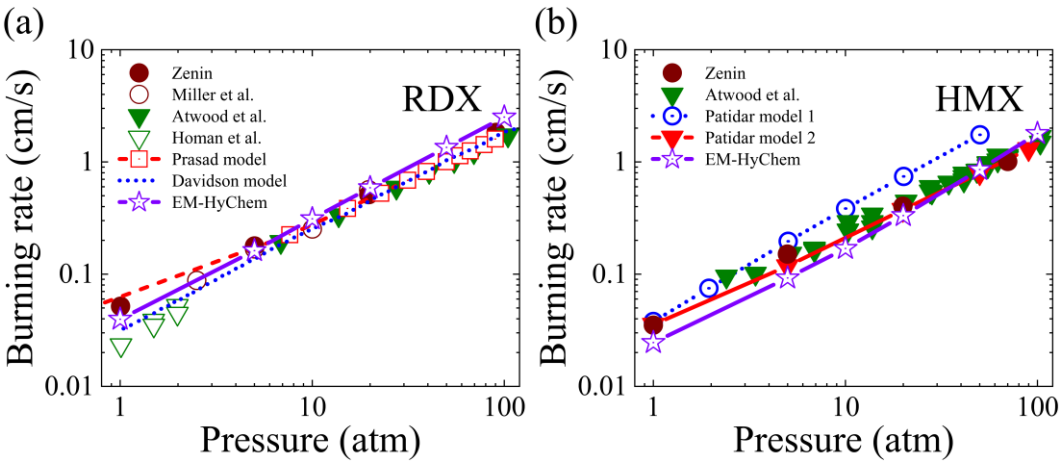

Figure 8. Burning rates predicted by the EM-HyChem model for (a) RDX and (b) HMX with experimental results or results from numerical simulations. The dots and lines represent the experimental values and numerical predictions, respectively. The Patidar model 1 and Patidar model 2 in Figure 8b consider a detailed condensed-phase reaction including 109 species and 157 reactions [21]. The gas-phase reactions of Patidar model 2 are consistent with those of the EM-HyChem model.

Simplified gas-phase mechanisms are employed to eliminate the macromolecular reactions associated with RDX and HMX. The corresponding prediction of the burning rate is consistent with the original gas-phase mechanisms for pressures higher than 10 atm (Figure S4). Considering the potential practical applications of the EM-HyChem approach, the gas-phase oxidation model can be further reduced to some extent because solid propellants typically operate at pressures higher than 20 atm, when the residual mass in the melt layer is expected to be negligible. The above point is also supported by heat flux analysis, as the key reactions contributing to the overall heat release are governed by the oxidation of pyrolysis fragments at pressures higher than 10 atm (Figure S5 and S6).

In addition to burning rates, other predicted combustion characteristics of the EM-HyChem model for RDX and HMX, including the temperature profile, melt layer thickness, and surface temperature, are compared with the experimental data and numerical results (Figure 9). In Figure 9(a), the predicted RDX temperature profile for spontaneous deflagration at ambient temperature and pressure is computed via the EM-HyChem model, with the findings of the Prasad and Liau models [5, 6]. The horizontal point at x=0 corresponds to the boundary of the melt layer and gas layer. The predicted temperature profile via the EM-HyChem model is more consistent than those via the other two models. The adiabatic flame temperature obtained by the Prasad model is ~3200 K, which is ~100 K higher than that predicted by the EM-HyChem and Liau models. The melt layer thicknesses of RDX at different pressures are also well reproduced by the EM-HyChem model compared with the Davidson model as well as the experimental data of Zenin [4, 44] at moderate pressures (< 20 atm). At high pressures (> 20 atm), both our model and the Davidson model underestimate the experimental values to some extent [4, 44]. Considering the surface temperature at the boundary between the melt layer and gas layer, the EM-HyChem model also makes good predictions across pressures from 1 to 100 atm, which aligns with the predictions of the Davidson model and exhibits a negligible discrepancy (~30 K) with experimental data from Zenin [4, 44]. Similarly, in Figure 9(b), the temperature distribution, melt layer thickness, and surface temperature of HMX are better captured by the EM-HyChem model than the methods of Patidar, Prasad, and Zenin [6, 44, 52] despite the underestimated burning rates at moderate pressures (<20 atm). The sensitivity of heat conduction in the melt layer to the above combustion characteristics, i.e., burning rate, melt layer thickness, and surface temperature, was also investigated to rule out their importance in the prediction (Figure S7). No obvious impact is shown in the cases of the burning rate and surface temperature, highlighting that a correct yet simple EM chemistry model is necessary for the excellent prediction of the above combustion characteristics. Therefore, the EM-HyChem model is capable of physically predicting the combustion characteristics during the combustion of solid materials.

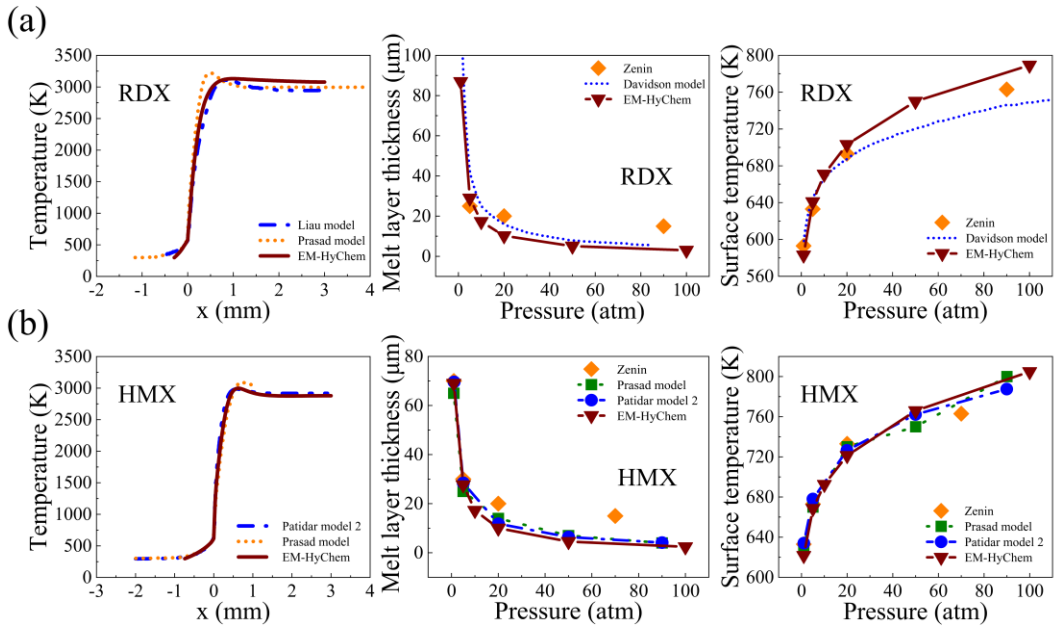

Figure 9. Predicted combustion characteristics via the EM-HyChem model for (a) RDX and (b) HMX: temperature profile at 1 atm (left), melt layer thicknesses at 1 to 100 atm (middle), and surface temperatures at 1 to 100 atm (left) compared with experimental results or other numerical results [4-6, 44, 52].

One-step lumped reactions have been extensively applied in past studies of EM decomposition and have prevailed for historic reasons, such as limited fitting capability and model simplicity. The EM-HyChem approach is a simplified modelling framework for deriving a one-step pyrolysis model together with an oxidation model for the pyrolysis products. Although it falls within the catalogue of one-step lumped reactions for pyrolysis, the two approaches are not the same in nature. First, the pyrolysis model is inspired by chemical intuition and supported by state-of-the-art NNP-enabled MD simulations. Second, the rate parameters of the pyrolysis model are derived from the modern NN enabled solver, which has a great fitting ability with limited computing costs. The above two points form a solid basis for the EM-HyChem approach and yield an alternative way to develop a physically based model with great generalizability and simplicity. Despite potential issues in the extension of the EM-HyChem approach to other critical systems in EMs, the value of the original HyChem approach in the combustion community has been demonstrated in various applications, including ignition [24, 25], flame speed [25, 27], extinction strain rate [26], and even kinetics in turbulent flows [59]. We believe that the EM-HyChem approach must inherit excellent adaptability from the pioneering work of the HyChem approach.

Conclusions

In this study, the reaction kinetics of the pyrolysis and oxidation reactions of RDX and HMX are modelled via MD simulations and a CRNN model in combination with the HyChem approach. Simplified submodels of the pyrolysis processes of RDX, HMX

and CL-20 are obtained, resulting in the following reactions: RDX => $3NO_2 + 3CH_2N$, HMX => $4NO_2 + 4CH_2N$ and CL-20 => $6NO_2 + 6CHN$. The subsequent oxidation of the pyrolysis products is constructed through the EM-HyChem model. On the basis of the EM-HyChem model, the burning rates across a wide range of pressure conditions are well predicted for RDX and HMX, exhibiting a high degree of consistency compared with experiments and previous models. Further validation of the EM-HyChem model from other combustion characteristics, including temperature profiles, melt layer thicknesses, and surface temperatures, is also demonstrated, thereby establishing a robust theoretical foundation and efficient computational means for the simulation of EMs. The success of the EM-HyChem model highlights its potential to resolve the complex reaction kinetics of EMs and offers a new direction for practical applications. Further extension of the EM-HyChem model for other EMs will be feasible in future studies.

Declaration of competing interests

The authors declare that they have no known competing financial interests or personal relationships that could have appeared to influence the work reported in this paper.

Acknowledgements

This work was supported by the State Key Laboratory of Explosion Science and Technology (Grant No. ZDKT21-01) and the National Natural Science Foundation of China (Grant No. 52106130). The authors also acknowledge support from the Foundation of Science and Technology on Combustion and Explosion Laboratory.

References

[1] D.M. Badgujar, M.B. Talawar, S.N. Asthana, P.P. Mahulikar, Advances in science and technology of modern energetic materials: An overview, J. Hazard. Mater. 151 (2008) 289-305. https://doi.org/10.1016/j.jhazmat.2007.10.039.

[2] P.F. Pagoria, G.S. Lee, A.R. Mitchell, R.D. Schmidt, A review of energetic materials synthesis, Thermochim. Acta. 384 (2002) 187-204. https://doi.org/10.1016/s0040-6031(01)00805-x.

[3] W.Q. Pang, C.Q. Deng, H. Li, L.T. DeLuca, D.H. Ouyang, H.X. Xu, X.Z. Fan, Effect of nanosnano-sized energetic materials (nEMs) on the performance of solid propellants: A review, Nanomaterials. 12 (2022) 17. https://doi.org/10.3390/nano12010133.

[4] J.E. Davidson, M.W. Beckstead, Improvements to steady-state combustion modeling of cyclotrimethylenetrinitramine, J. Propul. Power. 13 (1997) 375-383. https://doi.org/10.2514/2.5194.

[5] Y.C. Liau, V. Yang, Analysis of RDX monopropellant combustion with two-phase subsurface reactions, J. Propul. Power. 11 (1995) 729-739. https://doi.org/10.2514/3.23898.

[6] K. Prasad, R.A. Yetter, M.D. Smooke, An eigenvalue method for computing the burning rates of RDX propellants, Combust. Sci. Technol. 124 (1997) 35-82. https://doi.org/10.1080/00102209708935640.
[7] C. Rosères, L. Courty, P. Gillard, C. Boulnois, Burning velocities of pyrotechnic compositions: effects of composition and granulometry, Energies. 15 (2022) 10. https://doi.org/10.3390/en15113942.
[8] A.I. Atwood, T.L. Boggs, P.O. Curran, T.P. Parr, D.M. Hanson-Parr, C.F. Price, J. Wiknich, Burning rate of solid propellant ingredients, Part 1: Pressure and initial temperature effects, J. Propul. Power. 15 (1999) 740-747. https://doi.org/10.2514/2.5522.
[9] D. Chen, S.L. Huang, Q. Zhang, Q. Yu, X.Q. Zhou, H.Z. Li, J.S. Li, Two nitrogen-rich Ni(II) coordination compounds based on 5,5 ′ -azotetrazole: synthesis, characterization and effect on thermal decomposition for RDX, HMX and AP, RSC Adv. 5 (2015) 32872-32879. https://doi.org/10.1039/c5ra02464a.
[10] X.Z. Fan, J.Z. Li, Z.R. Liu, Thermal behavior of 1,1-diamino-2,2-dinitroethylene, J. Phys. Chem. A. 111 (2007) 13291-13295. https://doi.org/10.1021/jp075889l.
[11] J.S. Lee, C.K. Hsu, C.L. Chang, A study on the thermal decomposition behaviors of PETN, RDX, HNS and HMX, Thermochim. Acta. 392 (2002) 173-176. https://doi.org/10.1016/s0040-6031(02)00099-0.
[12] K. Wang, J.L. Wang, T.J. Guo, W. Wang, D.B. Liu, Research on the thermal decomposition kinetics and the isothermal stability of HMX, J. Therm. Anal. Calorim. 135 (2019) 2513-2518. https://doi.org/10.1007/s10973-018-7275-y.
[13] M. Khichar, Patidar, L.,Thynell, S., Comparative analysis of vaporization and thermal decomposition of cyclotrimethylenetrinitramine (RDX), J. Propul. Power. 35 (2019) 1098-1107. https://doi.org/10.2514/1.B37643.
[14] H.E. Kissinger, Variation of peak temperature with heating rate in differential thermal analysis, J. Res. Natl. Bur. Stand. 57 (1956) 217-221. https://doi.org/10.6028/jres.057.026.
[15] T. Ozawa, A new method of analyzing thermogravimetric data, Bull. Chem. Soc. Jpn. 38 (1965) 1881–1886. https://doi.org/10.1246/bcsj.38.1881.
[16] H.L. Friedman, Kinetics of thermal degradation of char-forming plastics from thermogravimetry. Application to phenolic plastic, J. polym. sci., C Polym. symp. 6 (1964) 183-195. https://doi.org/https://doi.org/10.1002/polc.5070060121.
[17] M.J. Starink, The determination of activation energy from linear heating rate experiments: A comparison of the accuracy of isoconversion methods, Thermochim. Acta. 404 (2003) 163-176. https://doi.org/10.1016/s0040-6031(03)00144-8.
[18] M. Fathollahi, B. Mohammadi, J. Mohammadi, Kinetic investigation on thermal decomposition of hexahydro-1,3,5-trinitro-1,3,5-triazine (RDX) nanoparticles, Fuel. 104 (2013) 95-100. https://doi.org/10.1016/j.fuel.2012.09.075.
[19] Q.J. Jiao, Y.L. Zhu, J.C. Xing, H. Ren, H. Huang, Thermal decomposition of RDX/AP by TG-DSC-MS-FTIR, J. Therm. Anal. Calorim. 116 (2014) 1125-1131. https://doi.org/10.1007/s10973-013-3621-2.

[20] Y. Tang, Z.-P. Li, H.-L. Zhou, C.-F. Miao, J.-C. Jiang, A.-C. Huang, Thermal stability assessment of nitrocellulose by using multiple calorimetric techniques and advanced thermokinetics, J. Therm. Anal. Calorim. 148 (2023) 5029-5038. https://doi.org/10.1007/s10973-022-11754-1.
[21] L. Patidar, M. Khichar, S.T. Thynell, A comprehensive mechanism for liquid-phase decomposition of 1,3,5,7-tetranitro-1,3,5,7-tetrazoctane (HMX): Thermolysis experiments and detailed kinetic modeling, Combust. Flame. 212 (2020) 67-78. https://doi.org/10.1016/j.combustflame.2019.10.025.
[22] D.P. Chen, K. Wang, H. Wang, Violation of collision limit in recently published reaction models, Combust. Flame. 186 (2017) 208-210. https://doi.org/10.1016/j.combustflame.2017.08.005.
[23] P. Zhang, S. Li, Y. Song, W. Shen, D. Chen, K. Wang, An experimental and modeling study on pyrolysis reaction kinetics of oxygenated biofuel blended with aviation kerosene RP-3, J. Anal. Appl. Pyrolysis. (2024) 106711. https://doi.org/https://doi.org/10.1016/j.jaap.2024.106711.
[24] H. Wang, R. Xu, K. Wang, C.T. Bowman, R.K. Hanson, D.F. Davidson, K. Brezinsky, F.N. Egolfopoulos, A physics-based approach to modeling real-fuel combustion chemistry - I. Evidence from experiments, and thermodynamic, chemical kinetic and statistical considerations, Combust. Flame. 193 (2018) 502-519. https://doi.org/10.1016/j.combustflame.2018.03.019.
[25] R. Xu, K. Wang, S. Banerjee, J.K. Shao, T. Parise, Y.Y. Zhu, S.K. Wang, A. Movaghar, D.J. Lee, R.H. Zhao, X. Han, Y. Gao, T.F. Lu, K. Brezinsky, F.N. Egolfopoulos, D.F. Davidson, R.K. Hanson, C.T. Bowman, H. Wang, A physics-based approach to modeling real-fuel combustion chemistry - II. Reaction kinetic models of jet and rocket fuels, Combust. Flame. 193 (2018) 520-537. https://doi.org/10.1016/j.combustflame.2018.03.021.
[26] Y.J. Tao, R. Xu, K. Wang, J.K. Shao, S.E. Johnson, A. Movaghar, X. Han, J.W. Park, T.F. Lu, K. Brezinsky, F.N. Egolfopoulos, D.F. Davidson, R.K. Hanson, C.T. Bowman, H. Wang, A Physics-based approach to modeling real-fuel combustion chemistry - III. Reaction kinetic model of JP10, Combust. Flame. 198 (2018) 466-476. https://doi.org/10.1016/j.combustflame.2018.08.022.
[27] K. Wang, R. Xu, T. Parise, J. Shao, A. Movaghar, D.J. Lee, J.W. Park, Y. Gao, T.F. Lu, F.N. Egolfopoulos, D.F. Davidson, R.K. Hanson, C.T. Bowman, H. Wang, A physics based approach to modeling real-fuel combustion chemistry - IV. HyChem modeling of combustion kinetics of a bio-derived jet fuel and its blends with a conventional Jet A, Combust. Flame. 198 (2018) 477-489. https://doi.org/10.1016/j.combustflame.2018.07.012.
[28] X. Tian, Song, S,Chen, F,Qi, X,Wang, Y,Zhang, Q, Machine learning-guided property prediction of energetic materials: Recent advances, challenges, and perspectives, Energetic Materials Frontiers. 3 (2022) 177-186. https://doi.org/https://doi.org/10.1016/j.enmf.2022.07.005.
[29] J.F. Rodrigues, Jr., L. Florea, M.C.F. de Oliveira, D. Diamond, O.N. Oliveira, Jr.,

Big data and machine learning for materials science, Discov Mater. 1 (2021) 12. https://doi.org/10.1007/s43939-021-00012-0.
[30] E. Heid, W.H. Green, Machine learning of reaction properties via learned representations of the condensed graph of reaction, J. Chem Inf. Model. 62 (2022) 2101-2110. https://doi.org/10.1021/acs.jcim.1c00975.
[31] W.Q. Ji, S.L. Deng, Autonomous discovery of unknown reaction pathways from data by chemical reaction neural network, J. Phys. Chem. A. 125 (2021) 1082-1092. https://doi.org/10.1021/acs.jpca.0c09316.
[32] L.L. Ye, Z.H. Zhang, F. Wang, X.D. Wang, Y.M. Lu, L. Zhang, Reaction mechanism and kinetic modeling of gas-phase thermal decomposition of prototype nitramine compound HMX, Combust. Flame. 259 (2024) 12. https://doi.org/10.1016/j.combustflame.2023.113181.
[33] Y.B. Xu, Q.Z. Chu, X.Y. Chang, H. Wang, S.K. Wang, S.L. Xu, D.P. Chen, Thermal decomposition mechanism of 1,3,5-trinitroperhydro-1,3,5-tria- zine: Experiments and reaction kinetic modeling, Chem. Eng. Sci. 282 (2023) 12. https://doi.org/10.1016/j.ces.2023.119234.
[34] H. Wang, Y.B. Xu, M.J. Wen, W. Wang, Q.Z. Chu, S. Yan, S.L. Xu, D.P. Chen, Kinetic modeling of CL-20 decomposition by a chemical reaction neural network, J. Anal. Appl. Pyrolysis. 169 (2023) 11. https://doi.org/10.1016/j.jaap.2023.105860.
[35] W. Sun, Y. Xu, X. Chen, Q. Chu, D. Chen, Kinetic models of HMX decomposition via chemical reaction neural network, J. Anal. Appl. Pyrolysis. 179 (2024) 106519. https://doi.org/https://doi.org/10.1016/j.jaap.2024.106519.
[36] M.W. Beckstead, K. Puduppakkam, P. Thakre, V. Yang, Modeling of combustion and ignition of solid-propellant ingredients, Prog. Energy Combust. Sci. 33 (2007) 497-551. https://doi.org/10.1016/j.pecs.2007.02.003.
[37] M. Jeppson, M. Beckstead, Q. Jing, A kinetic model for the premixed combustion of a fine AP/HTPB composite propellant, 36th AIAA Aerospace Sciences Meeting and Exhibit, American Institute of Aeronautics and Astronautics.
[38] M.L. Gross, Two-Dimensional Modeling of AP/HTPB Utilizing a Vorticity Formulation and One-Dimensional Modeling of AP and ADN, Ira A. Fulton College of Engineering and Technology; Chemical Engineering, Brigham Young University - Provo, 2007.
[39] D.G. Goodwin, H.K. Moffat, R.L. Speth, Cantera: An Object-oriented Software Toolkit for Chemical Kinetics, Thermodynamics, and Transport Processes. https://zenodo.org/records/1174508, 2018 (Accessed 24 August 2018).
[40] M.W. Beckstead, R.L. Derr, C.F. Price, A model of composite solid-propellant combustion based on multiple flames, AIAA J. 8 (1970) 2200-2207. https://doi.org/10.2514/3.6087.
[41] M.S. Miller, In Search of an Idealized Model of Homogeneous Solid-Propellant Combustion, Combust. Flame. 46 (1982) 51-73. https://doi.org/10.1016/0010-2180(82)90006-2.
[42] M.S. Miller, W.R. Anderson, Burning-rate predictor for multi-ingredient

propellants: Nitrate-ester propellants, J. Propul. Power. 20 (2004) 440-454. https://doi.org/10.2514/1.10386.
[43] M.S. Miller, W.R. Anderson, Energetic-Material Combustion Modeling with Elementary Gas-Phase Reactions: A Practical Approach, Solid Propellant Chemistry, Combustion, and Motor Interior Ballistics, American Institute of Aeronautics and Astronautics, U.S. Army Research Laboratory, Aberdeen Proving Ground, Maryland, 2000, pp. 501-531.
[44] A. Zenin, HMX and RDX - Combustion Mechanism and Influence on Modern Double-Base Propellant Combustion, J. Propul. Power. 11 (1995) 752-758. https://doi.org/10.2514/3.23900.
[45] G. Lengellé, J. Duterque, J.F. Trubert, Combustion of solid propellants RTO/VKI Special Course on "Internal Aerodynamics in Solid Rocket Propulsion". (2002). https://doi.org/doi:10.2514/3.55069.
[46] M.J. Wen, X.Y. Chang, Y.B. Xu, D.P. Chen, Q.Z. Chu, Determining the mechanical and decomposition properties of high energetic materials (α-RDX, β-HMX, and ε-CL-20) using a neural network potential, Phys. Chem. Chem. Phys. 26 (2024) 9984-9997. https://doi.org/10.1039/d4cp00017j.
[47] B.W. Hamilton, P. Yoo, M.N. Sakano, M.M. Islam, A. Strachan, High-pressure and temperature neural network reactive force field for energetic materials, J. Chem. Phys. 158 (2023) 12. https://doi.org/10.1063/5.0146055.
[48] Z.H. Zhang, L.L. Ye, X.D. Wang, X.G. Wu, W. Gao, J.Z. Li, M.S. Bi, Unraveling the reaction mechanism on pyrolysis of 1,3,5-trinitro-1,3,5-triazinane (RDX), Combust. Flame. 242 (2022) 12. https://doi.org/10.1016/j.combustflame.2022.112220.
[49] L. Martínez, R. Andrade, E.G. Birgin, J.M. Martínez, Packmol: a package for building initial configurations for molecular dynamics simulations, J. Comput. Chem. 30 (2009) 2157-2164. https://doi.org/10.1002/jcc.21224.
[50] G. Tang, H. Wang, C.Y. Chen, Y.B. Xu, D.P. Chen, D.L. Wang, Y.J. Luo, X.Y. Li, Thermal decomposition of nano Al-based energetic composites with fluorinated energetic polyurethane binders: experimental and theoretical understandings for enhanced combustion and energetic performance, RSC Adv. 12 (2022) 24163-24171. https://doi.org/10.1039/d2ra03781e.
[51] Y. Xu, Q. Chu, D. Chen, A reaction kinetic model of nano Al-PTFE composite from chemical reaction neural networks, Chin J Explos Propellants. 44 (2021) 800-810. https://doi.org/10.14077/j.issn.1007-7812.202108038.
[52] L. Patidar, LalitPatidar/solid-propellant-combustion-model. https://github.com/LalitPatidar/solid-propellant-combustion-model, 2019 (Accessed 2019/12/12).
[53] W.J. Pitz, C.K. Westbrook, A detailed chemical kinetic model for gas phase combustion of TNT, Proc. Combust. Inst. 31 (2007) 2343-2351. https://doi.org/10.1016/j.proci.2006.08.061.
[54] B.E. Homan, M.S. Miller, J.A. Vanderhoff, On the flame structure of RDX, PN, 2001.

[55] L. Patidar, M. Khichar, S. Thynell, Modeling of HMX monopropellant combustion with detailed condensed-phase kinetics, AIAA Propulsion and Energy 2019 Forum, American Institute of Aeronautics and Astronautics, The Pennsylvania State University, 2019.
[56] T.B. Brill, Multiphase chemistry considerations at the surface of burning nitramine monopropellants, J. Propul. Power. 11 (1995) 740-751. https://doi.org/10.2514/3.23899.
[57] S.T. Thynell, P.E. Gongwer, T.B. Brill, Condensed-phase kinetics of cyclotrimethylenetrinitramine by modeling the T-jump/infrared spectroscopy experiment, J. Propul. Power. 12 (1996) 933-939. https://doi.org/10.2514/3.24125.
[58] D. Chakraborty, R.P. Muller, S. Dasgupta, W.A. Goddard, A detailed model for the decomposition of nitramines: RDX and HMX, J. Comput-Aided Mater. Des. 8 (2001) 203-212. https://doi.org/10.1023/A:1020074113000.
[59] L. Esclapez, P.C. Ma, E. Mayhew, R. Xu, S. Stouffer, T. Lee, H. Wang, M. Ihme, Fuel effects on lean blow-out in a realistic gas turbine combustor, Combust. Flame. 181 (2017) 82-99. https://doi.org/https://doi.org/10.1016/j.combustflame.2017.02.035.